

Transparent and Efficient Solar Windows TES-W



Final report (confidential)

Project details

Projectnumber: TEUE 1921203
Project title: Transparent and Efficient Solar Windows
Coordinator: Universiteit Utrecht
Partners: Physee
Project period: 1 April 2021 – 1 October 2023

Contact details

This report is created by the project partners: Utrecht University and Physee. For questions regarding the project, results, and follow-up projects you can contact:

Universiteit Utrecht

Wilfried van Sark

+31 30 2537611

w.g.j.h.m.vansark@uu.nl

Authors

Wilfried van Sark, Thomas de Bruin, Raimon Terricabres Polo, Celso de Mello Donega (UU), Pim Rutgers, Joe Kao (Physee)

Subsidy

The project was supported with a subsidy from the Dutch Ministry of Economic Affairs, National EZ subsidies, Topsector Energie, performed by the Rijksdienst voor Ondernemend Nederland (RVO).

Acknowledgements

We would like to explicitly like to thank Annanta Kaul, Anne de Waal, Sander Deelen, Jody Wisman, Tim Prins, Daniel Vanmaekelbergh (UU), Dick de Boer (Solumineus), Veronique Gevaerts, Henk Steijvers, Minne de Jong, Maarten Dörenkämper (TNO), Stijn Verkuilen, Walter Groenewoud (Heijmans), Rob van Kemenade (Rovake) and Jeroen ter Schiphorst (Lusoco) for their contributions.

Cover

The picture on the cover © Thomas de Bruin.

Summary

Near Zero Energy Buildings will be required in the near future that generate a substantial part of their electricity demand by renewables. For tall buildings, photovoltaic (PV) systems will not generate sufficient electricity. Opaque or transparent building-integrated PV façades are indispensable, but efficiency of transparent PV is yet too low.

The goal of this project was to develop transparent solar windows with transparency >60% in the visible part of the solar spectrum with 5% energy conversion efficiency, using the principle of luminescent solar concentrators (LSCs). Nano-sized luminescent species have been developed that show high photoluminescence quantum yield and limited re-absorption loss.

The luminescent species have been used in a double polymer plate sandwich structure combined with solar cell strips on the sides of the structure, thus creating a luminescent solar concentrator. These highly transparent LSCs were subjected to indoor and 1-year outdoor tests which showed that their energy conversion efficiency is less than 1%. This low efficiency is most probably due to prototype design issues including shunt resistance loss in the solar cells and can thus be increased by improved design. Stability analyses have revealed that some of the luminescent species used in the LSCs lead to either an increase or a decrease in efficiency, which can be explained by photodarkening and photobrightening effects.

Computer simulations have explored optimum solar window designs and luminescent species which, after experimental validation can increase the TRL closer to commercialization.

Preface

This final report describes the work performed in the project TES-W (Transparent and Efficient Solar Windows) as carried out within the framework of the Nationale regelingen EZ-subsidies, Topsector Energie, executed by the Rijksdienst voor Ondernemend Nederland. The report addresses the results obtained. In addition, several project changes are described.

Contents

Summary.....	3
Preface.....	4
Contents	5
1. Introduction.....	6
2. Project set-up	9
3. Results	10
3.1. Nanoparticles.....	10
3.2. Devices.....	13
3.2.1. Modeling.....	13
3.2.2. Prototypes	17
3.3. Testing	19
3.3.1. Indoor.....	19
3.3.2. Outdoor.....	21
4. Discussion	29
5. Follow up activities	30
6. Dissemination	31
References.....	34

1. Introduction

Building-Integrated Photovoltaics (BIPV) has been emerging in recent years with a strong emphasis on aesthetics while at the same time focusing on decreasing cost and optimizing energy performance [1]. To reduce greenhouse gas emissions in the built environment, Near Zero Energy Buildings (NZEBS) are required that generate a substantial part of their energy usage decentralised through renewable sources. Especially regarding multi-story buildings, roof area is too small to generate enough energy by means of conventional photovoltaic (PV) systems added on the roof. BIPV elements on façades are indispensable for these buildings. Besides the present development of opaque façade elements based on conventional silicon-based PV modules that are colourful and/or show a printed design, windows make a large part of the façade. Especially modern office buildings can have completely glass-based building envelopes. Thus, transparent PV (TPV) components need to be developed, where transparency level and energy yield are contrasting optimization parameters.

The field of TPV is emerging fast, with examples such as organic PV and amorphous silicon PV [2]. An alternative technology and material system that is investigated in TPV is based on the luminescent solar concentrator principle. The window itself is absorbing part of the incoming solar irradiation of which a part is harvested in solar cells at the side of the window using luminescent species (luminophores) in the window (see Figure 1). Up to now, highly transparent, colourless windows based on the LSC principle have a poor efficiency of less than 1% [2]. Research activities thus focus on increasing this efficiency, while maintaining the high transparency. This is possible as transparency is required only in the visible part of the solar spectrum ($435 \text{ nm} < \text{VIS} < 670 \text{ nm}$), thus, ideally, using luminophores that absorb all UV

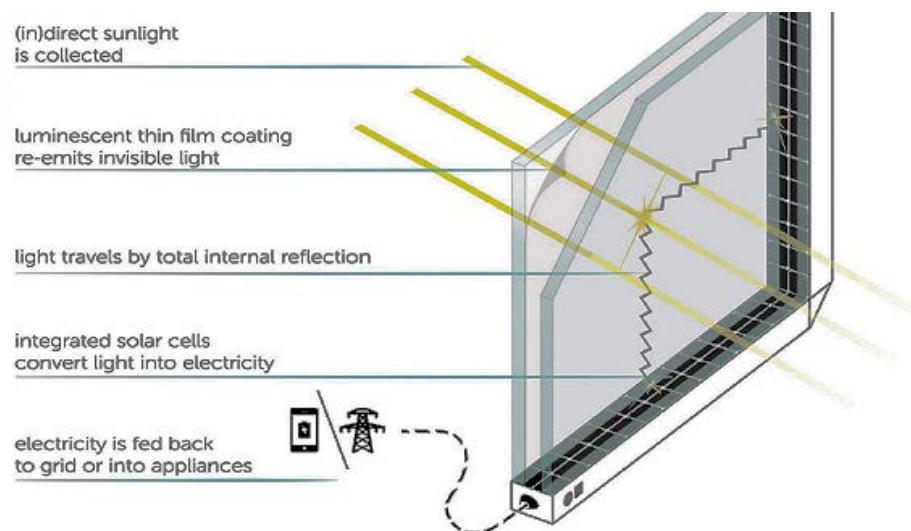


Figure 1. Principle of LSC solar window.

(<435 nm) and NIR (>670 nm), will increase conversion efficiency, without affecting transparency in the visible. Assuming full UV and NIR absorption (until 1100 nm) and 20% of the visible spectrum, the maximum theoretical photon conversion efficiency (PCE) is 20%, using silicon solar cells attached to the sides.

Major challenges in LSC research are 1) to achieve a high photoluminescence quantum efficiency (or yield, PLQY) of luminophores, that is, the efficiency of emitting an absorbed photon should be above 90%, and 2) to realize close-to-zero self-absorption which is due to the overlap of emission and absorption spectrum. In addition, the solar cell attached to the sides should have high external quantum efficiency (EQE) in the emission range of the luminophores.

This project has developed several LSC-based solar windows with transparency >60% in the visible part of the solar spectrum. The targeted energy conversion efficiency of 5% was not reached, however reasons for that were investigated using extensive computer simulations.

In more detail, several luminophore candidate materials systems have been investigated, including CuIn(S)/ZnS (CIS core/shell) nanocrystals (NCs), as they show appreciable UV and NIR absorption with limited VIS absorption as shown in Figure 2 [3]. The NCs are dispersed in coatings on glass or embedded in a polymer such as polymethylmethacrylate (PMMA) to allow the fabrication of LSCs. Transparency depends on the concentration of NCs in the LSC. Optimization of NCs was targeted at achieving high PLQY and minimal self-absorption, and highest possible PCE at certain transparency (between 60 and 80%).

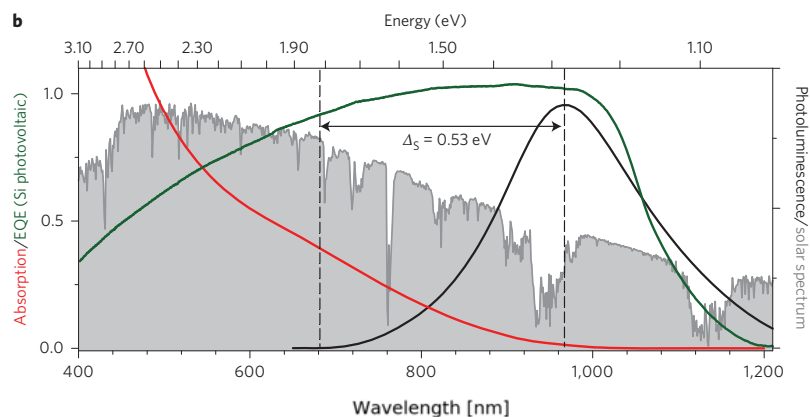


Figure 2. Absorption and emission spectrum of CIS nanocrystals in comparison to the AM1.5 solar spectrum [3].

CIS NCs can be synthesized presently at UU with PLQY>80% and NC size of 4-5 nm [4]. For these CIS NCs, crystalline Si (c-Si) cells would be suitable to be attached on the LSC sides as they are converting photons of up to 1050 nm wavelength. However, we used CIGS cells with potential lower bandgap as this allows to also target CIS NCs with emission further into the NIR.

The resulting LSCs were highly transparent but coloured since CIS NCs absorb also in the visible. Therefore, the visual appearance of the LSCs was investigated using the CIE chromaticity diagram. Figure 3 shows earlier (modelling) work from which it can be inferred that LSCs with embedded CIS NCs appear yellowish-orange at high transparency. However, correlated colour temperatures (CCT) and colour rendering index (CRI) are high [5]. This means that potential visual discomfort indoors, for persons behind the window, is minimal.

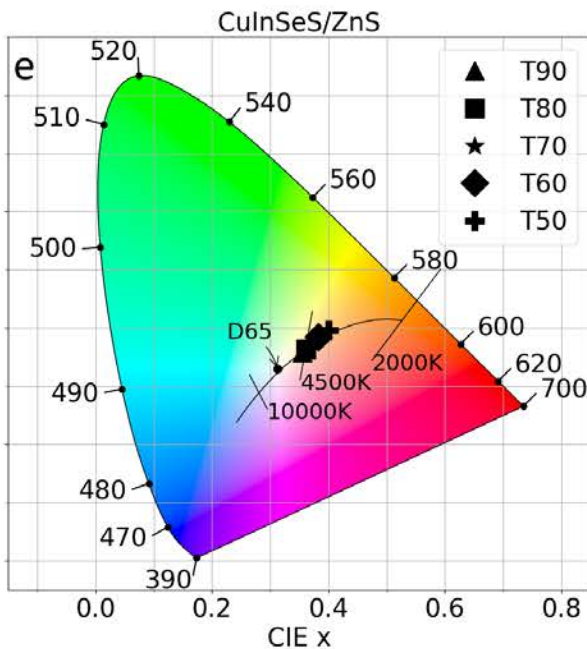


Figure 3. Chromaticity diagram for CIS NCs coating on glass [5].



Figure 4. Photograph of LSC with CdSe/ZnS NCs, during the attachment of solar cell strips at UU.

To facilitate efficient laboratory work, we note that computer simulations using ray-trace simulations based on Monte Carlo principles were used to guide the experiments by optimizing LSCs based on candidate luminophores in terms of concentration, thus optimizing absorption, transparency, and PCE.

At the moment, nanocrystal based LSC prototypes are at TRL3/4, see, e.g., Figure 4, based on our earlier work. For other luminophores, an LSC demonstrator with single luminescent species (organic dye) is at TRL 7, as evidenced by the Solar Noise Barrier project [6] and the Electric Mondrian prototype [7].

2. Project set-up

The project was divided in five work packages (WPs). Every work package is further subdivided in several tasks (T). Project management and dissemination is performed in WP1. WP2 (nanoparticle optimization) contains two tasks in which first nanoparticle materials are selected after which they are synthesized. In WP3 (prototype development) results of WP2 are used in the design of the prototype (Task 3.1) followed by the realization of the design. Indoor and outdoor testing is pursued in WP4. Results from WPs 2, 3 and 4 are used in defining a business case strategy. A short breakdown is provided below, with WP/task leaders in bold and durations are indicated as well in months. Project duration was three years.

WP 1: Project management (Month 1 – Month 30) (UU)

T1.1 Project meetings (M1-M30) (UU)

T1.2 Dissemination (M4-M30) (UU)

WP 2: Nanoparticle optimization (Month 1 – Month 12) (UU)

T2.1 Selection of nanoparticles (M1-M3) (UU)

T2.2 Synthesis of nanoparticles (M3-M12) (UU)

WP 3: Prototype development (Month 7 – Month 18) (Physee)

T3.1 Selection of designs (M7-M14) (UU)

T3.2 Realization of designs (M12-M18) (Physee)

WP 4: Performance testing (Month 13 – Month 30) (UU)

T4.1 Indoor STC testing (M13-M20) (Physee)

T4.2 Outdoor testing (M18-M30) (UU)

WP 5: Business case design (Month 25 – Month 30) (Physee)

T5.1 Business plan for future exploitation (M25-M30) (Physee)

3. Results

3.1. Nanoparticles

The selection of nanoparticles was performed based on the initial candidates CIS and barium phosphate. The focus of the work was on reaching high quantum efficiency (>90%) and minimal self-absorption loss as evidenced by minimal overlap between emission and absorption spectra. A literature study establishing latest results regarding state-of-the-art in combination with expertise at UU/Debye and Physee led to the choice of developing best recipes for synthesis of CIS nanocrystals only, and to explore quantum cutting perovskites, i.e., Yb³⁺-doped CsPbX₃ (X = Cl, Br) NCs, as they can potentially reach 200% photoluminescence quantum yield (PLQY) [8]. Barium phosphate micro-sizes particles were not further investigated because it was found that their quantum efficiency would be too low (<30%) to realize efficient LSC-based windows, especially in combination with scattering losses.

CuInS₂ NCs were synthesized following two different synthetic routes, yielding two different crystal types:

- 1) Heating-up method to obtain CuInS₂ NCs with the chalcopyrite (cp) phase [9]
- 2) Cu for In cation exchange in Cu₂S NCs to obtain CuInS₂ NCs in the wurtzite (wz) phase [4]

The first method allowed for straightforward gram-scale production of nanocrystals, where the heating time determines the particle size and, hence, the optical properties. The synthesized NIR emitting cp CuInS₂ NCs were however of insufficient quality because the long reaction times needed for their formation resulted in colloidal instability and broad size dispersion. This issue is very detrimental to the LSC performance, since the larger particles will reabsorb more light (Figure 5A). To circumvent these limitations, the second synthetic method was followed, which allows for a precise size control of the product (Figure 5B). The synthesis of wz CuInS₂ NCs emitting in the 1.3-1.1 eV (950-1130 nm) range was successful (Figure 6B). The cation exchange process was optimized to ensure that the product NCs were stable in solution. We found that the addition of small amount of trioctylphosphine (TOP), the ligand assisting the cation exchange, was essential to stabilize the NCs in solution and enhance the luminescence (Figure 6) [10].

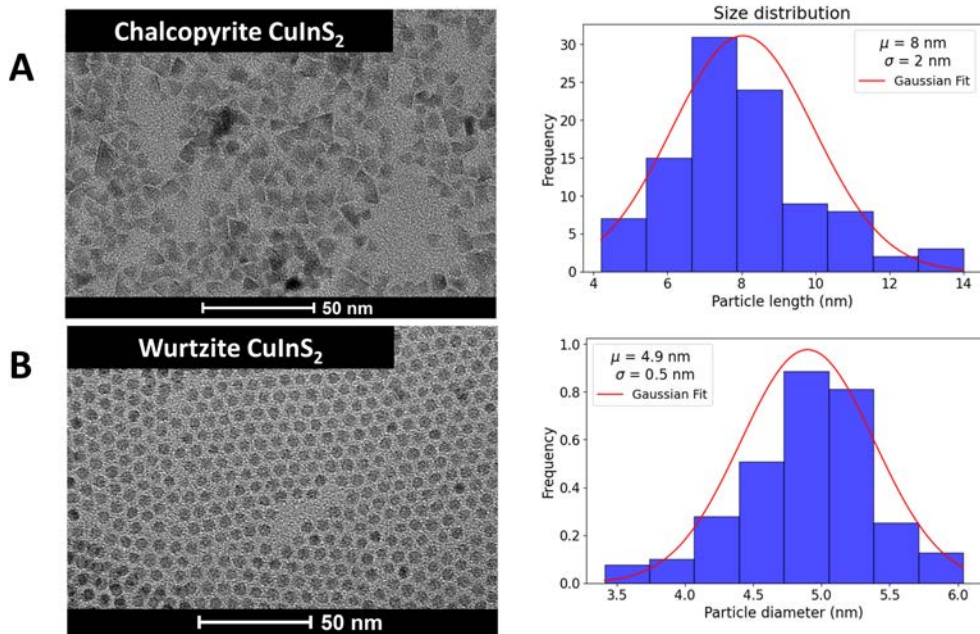


Figure 5. TEM images and size distribution histograms of (A) chalcopyrite CuInS_2 NCs and (B) wurtzite CuInS_2 NCs. Note the coefficient of variation is much larger in the chalcopyrite phase product (25%) than the wurtzite one (10%).

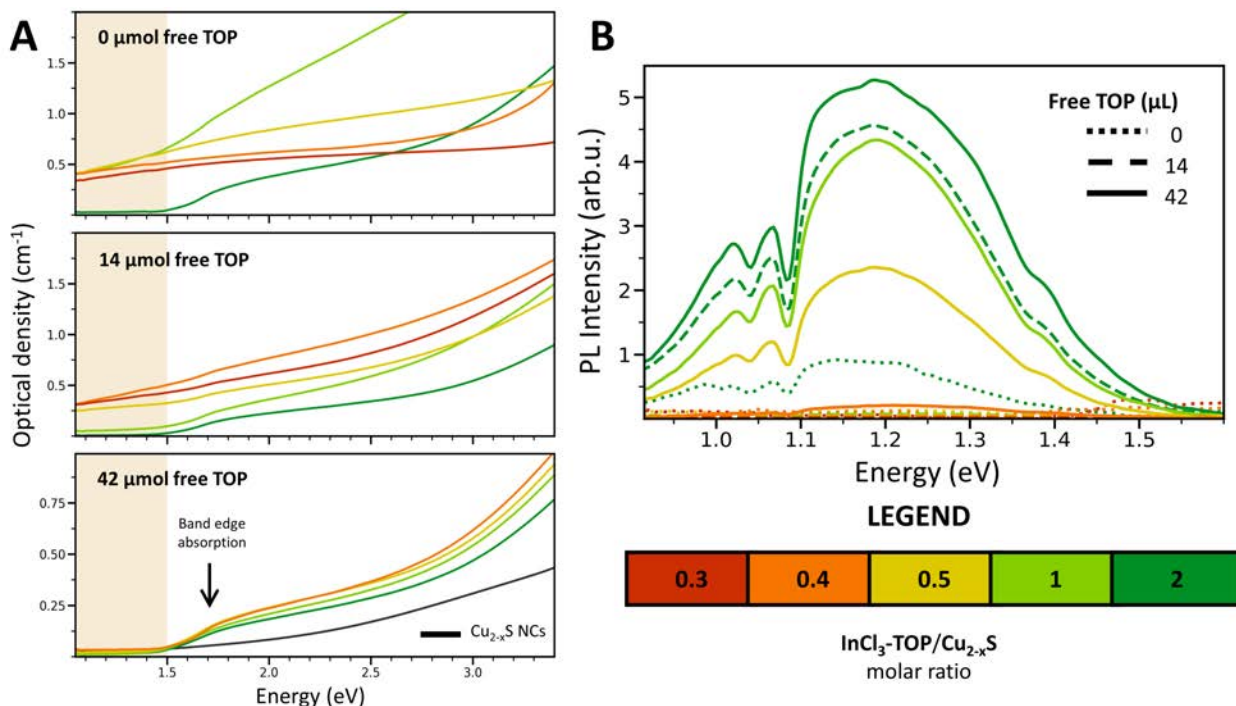


Figure 6. Absorption (A) and emission (B) spectra of wurtzite CuInS_2 NCs obtained using different amounts of precursor (color code) and additional amount of the ligand TOP.

To improve the luminescence of the product NCs, several post-synthetic modifications were investigated. Most of the efforts focused on the incorporation of Ga^{3+} in the NCs by cation exchange.

The motivations behind are:

- 1) increase the PLQY [11],
- 2) facilitate the growth of a ZnS shell while preventing Zn^{2+} diffusion inwards (surface depleted of Cu^+),
- 3) modulate the bandgap of the NCs with the Ga^{3+} content.

The incorporation of Ga^{3+} in both cp and wz CuInS_2 NCs was successful but the process proved difficult to control. The incorporation of Ga^{3+} and the corresponding increase in PLQY and blueshift in the bandgap was confirmed (Figure 7). Studies exploring the reaction conditions (time, temperature, concentration of reagents) and the surface of the NCs (washing method, use of ligands) were unsuccessful in devising a reproducible and robust protocol.

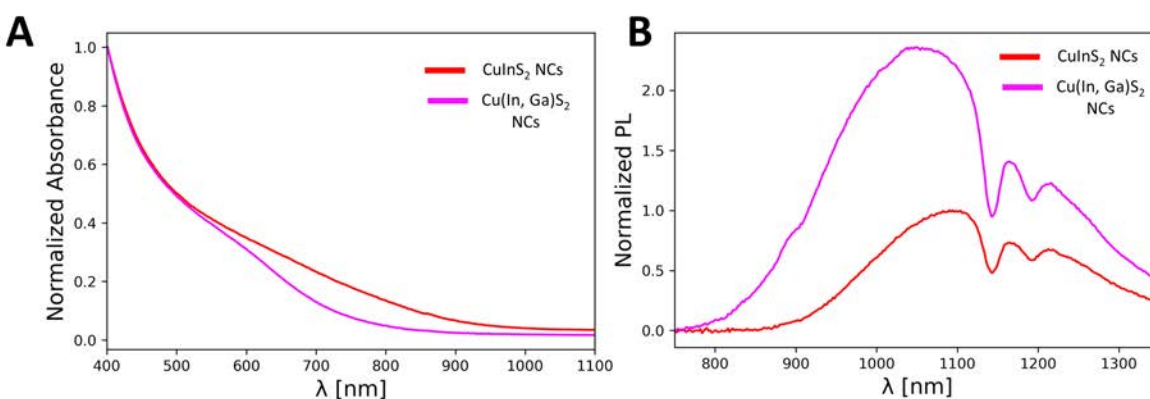


Figure 7. Absorption (A) and emission (B) of cp CuInS_2 NCs before and after incorporation of Ga^{3+} . The atomic ratios were 0.53:0.43:1 (Cu:In:S) and 0.25:0.16:0.38:1 (Cu:Ga:In:S) for the template and Ga-rich NCs, respectively.

For small cp CuInS_2 NCs (<2 nm) (limited) incorporation of Ga^{3+} had no observable impact on the diffusion of Zn^{2+} into the NCs and the formation of graded alloy $(\text{Cu,In,Zn})\text{S}_2$ NCs. Apart from the Ga^{3+} incorporation, ZnS and CdS shells were successfully overgrown on CuInS_2 NCs, yielding samples with PLQYs of 20% and 60%, respectively. Current research focuses on further improving the PLQY values while avoiding Cd-based reagents by optimizing the shelling reaction.

In recent years, quantum cutting perovskites have become promising luminophores for photovoltaic applications [8]. Motivated by the potential gains of up to 200% PLQY, we investigated the synthesis of Yb^{3+} -doped CsPbX_3 ($X = \text{Cl, Br}$) NCs. The synthesis of NIR-emitting perovskites was successful, albeit with low PLQY (<10%) (Figure 8).

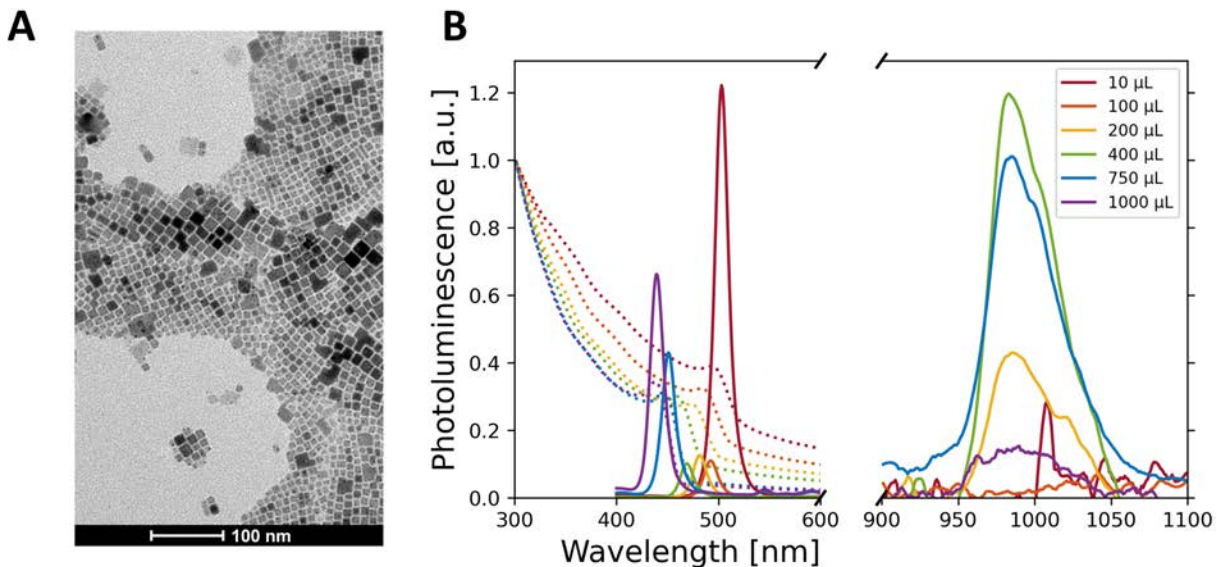


Figure 8. (A) TEM image of the synthesized CsPbBr_3 NCs. (B) Absorption (dashed line) and emission (solid line) spectra of Yb^{3+} -doped CsPbBr_3 upon the addition of different amount of Cl precursor (see color code).

3.2. Devices

3.2.1. Modeling

Before the development of LSC prototype devices it is useful to use modelling software to fine tune parameters in order to obtain the most effective device. An LSC is most useful if the transmitted light allows for pleasant working conditions, while the maximum amount of electricity is being generated. The LSC suffers from an inherent trade-off between transparency and electricity generation thus optimizing this will lead to the most effective devices.

The lowest transparency of an LSC that still allows for pleasant working environments was presented by Traverse et al. [2]. They propose that a transparent solar cell used as energy harvesting window should have a colour rendering index (CRI) of 70 or higher, and an average visible transmittance (AVT) of 55% or higher.

Modeling LSCs has been used for various luminophores and concentrations, waveguide material, and dimensions. Historically, two types of LSC models have been developed, thermodynamic models with a focus on fluorescent dyes [12,13] and quantum dots (QD) [14] and Monte Carlo based ray trace models encompassing both types of luminophores [15-18], see Figure 9 for an impression for a triple LSC

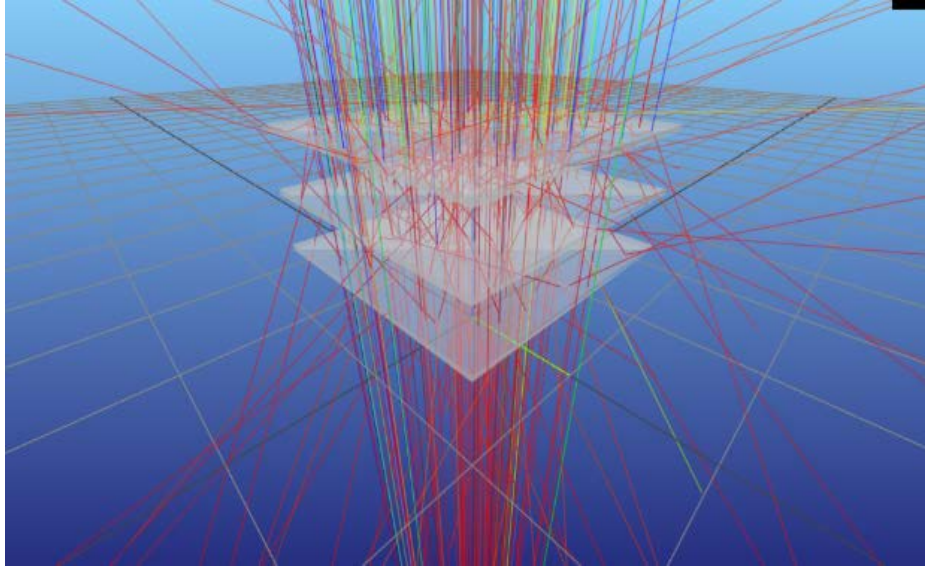


Figure 9. Visual representation of PVtrace [17] generating 200 rays emitted from a square light AM1.5G spectrum incident on three LSC panels. The figure shows the light being emitted to the sides and shifted to red wavelengths [12].

structure [19]. The advantage of ray trace modeling is the flexibility and ease of use, while the thermodynamic models are much faster.

Using raytracing, LSC device optimization in terms of PCE while imposing constraints at AVT and/or CRI has been performed [20]. This has been done for ideal luminophores, i.e., absorbing fully in the UV and NIR, and only up to certain levels in the visible, which thus determines AVT. Figure 10 shows modelled

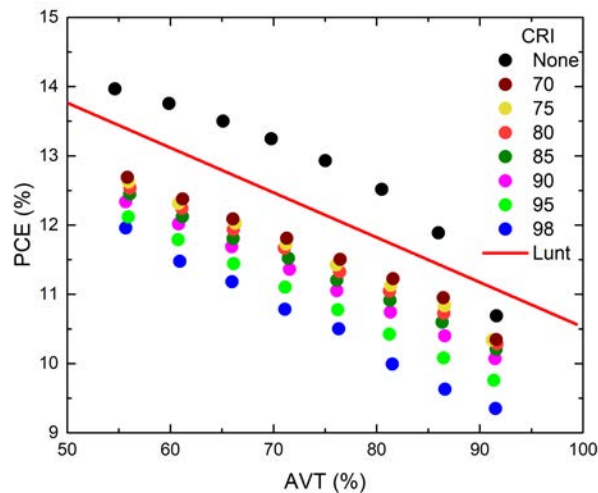


Figure 10. PCE as a function of AVT for different CRI constraints in LSC modeling [20]. "None" refers to simulations without imposing constraints on CRI. Values from Lunt [21] are based on the practical limit values in Fig. 3b in his paper.

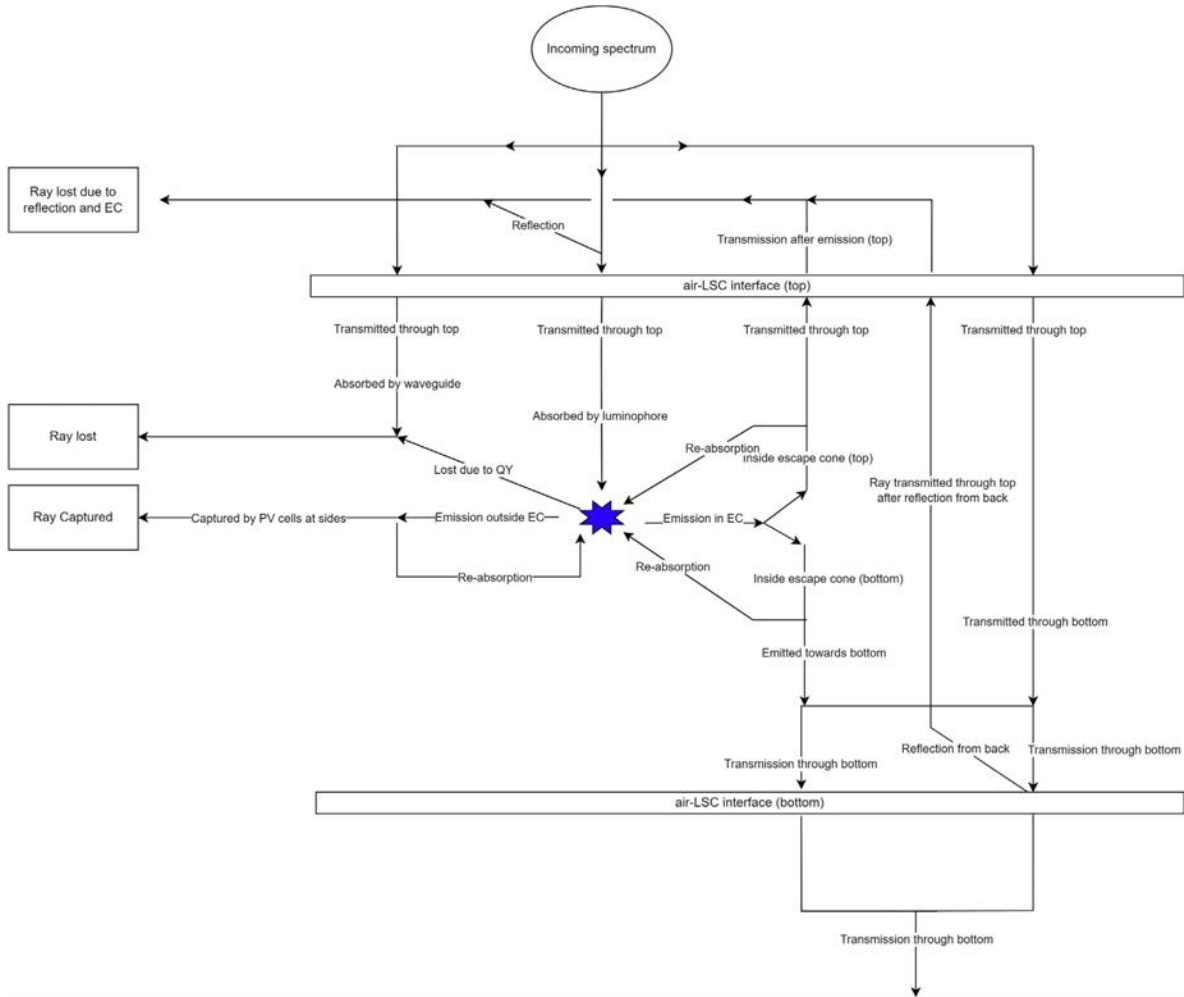


Figure 11. Flowchart of possible routes a ray of light can take within an LSC. Note that the arrows indicate a possible path, and the thickness or length of the arrows has no meaning. Furthermore, the absorption by a luminophore after reflection from the back of an LSC is not incorporated. The reflection is only incorporated to account for a decrease in the transmission of the incoming spectrum [23].

PCE as a function of AVT for 7 different CRI values used as constraint, and for the unconstrained cases. It is found that PCE decreases for increasing AVT. Still, for AVT = 80% and CRI =90 (excellent transparency and colour rendering properties), PCE can be near 11%. In the same graph the results from calculations of Lunt [21] are shown, for so-called realistic LSC conditions, including various optical losses. The CRI constrained results show lower PCE for higher values of CRI, and the unconstrained case shows highest PCE, at AVT<90%.

Figure 11 shows the flowchart of possible routes that a ray of light can take in the LSC, which are incorporated in the ray-trace simulations. As these simulations require substantial time, a novel algorithm is developed that is able to calculate the optimal balance between transparency and electricity

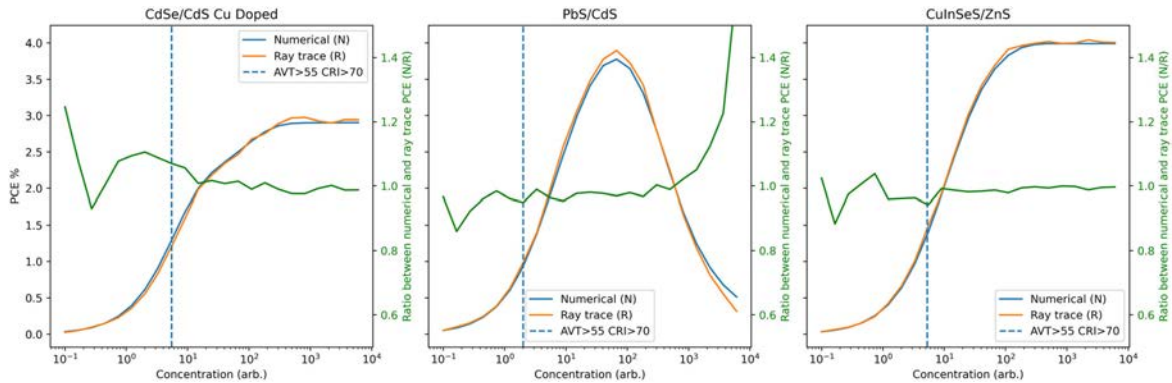


Figure 12. PCE of the tested luminophores. Left of the blue line shows concentration values leading to an AVT above 55% and a CRI above 70. The green line (right y-axis) indicates the ratio between numerical and ray trace PCE results. The algorithm deviates at lower concentrations due to insufficient rays for low-probability events.

generation for rectangular LSC devices of any size and for any luminophore. The algorithm is based on the analytical description of an LSC as proposed by Sychugov [22]. In his paper he calculates the probability density function of the path lengths that occur after emission by the luminophore. This function is dependent on the LSC dimensions, the absorbance, and the refractive index of the waveguide. We used his function to replace the time-consuming ray tracing thus creating a numerical algorithm that allowed for greater flexibility as well as a more detailed result. A detailed mathematical description is given in [23].

The validation of the new method has been done by comparing it with ray trace simulations. For that we used a rectangular PMMA LSC of $8 \times 4 \text{ cm}^2$ with a thickness of 0.5 cm, for three different cases of NCs, i.e., CdSe/CdS Cu doped (QY=70%) [24], PbS/CdS (QY = 50%) [25], and CuInZnS/ZnS (QY = 50%) [3]. Figure 12 shows the PCE results for the ray trace algorithm and the numerical algorithm for the tested luminophores. The green line in the figure shows the ratio of numerical and ray trace PCE results, which is close to 1 for most concentration values. Another validation result is linked to scalability of LSCs. Figure 13 shows the results for square dimensions (13A), the rectangular dimensions (13B), and the thickness (13C).

Good correspondence between ray trace and numerical results is clear. Figure 13A,B shows the well-known result that larger LSCs have lower PCE, while PCE stabilized for sizes larger than 1 m. For Figure 13C, the numerical and ray trace methods deviate at higher thicknesses. This is probably due to a 2D approximation used in the model which becomes less accurate for higher thicknesses [23].

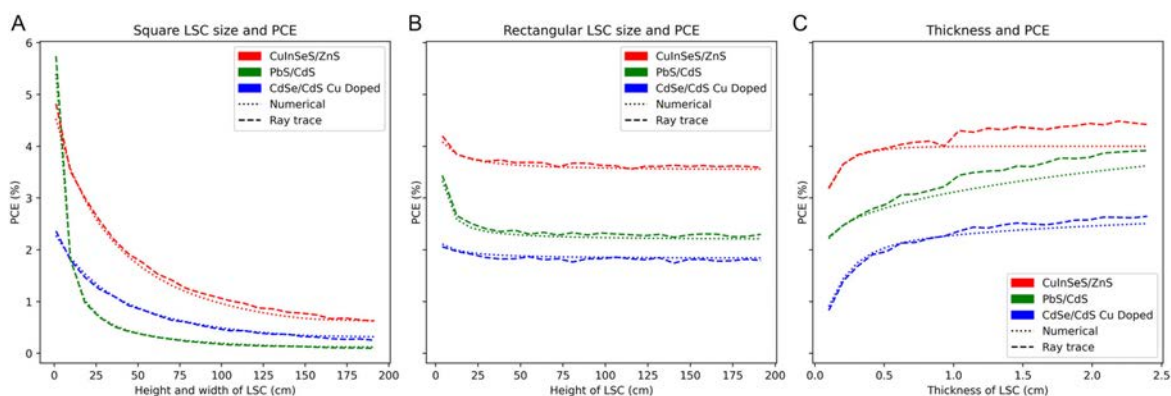


Figure 13. PCE results for the three tested luminophores for different A) square LSC dimensions ($h = 1/4 w$) in cm, B) LSC heights (h), starting from 4.0 to 200 cm, while the LSC width (w) is kept constant at 4.0 cm. C) Thickness of $8 \times 4 \text{ cm}^2$ LSC. Refractive indices of air and PMMA are 1.0 and 1.5, respectively, in all figures.

We found that for the transparency constraints as defined above ($AVT > 55\%$, $CRI > 70$), the maximum obtainable PCE is around 1% for currently existing luminophores. This indicates that significant technological breakthroughs are necessary for LSCs to become economically viable which happens, as speculated, around the 5% efficiency mark. Breakthroughs can occur via improved luminophore characteristics with for instance quantum-cutting luminophores [8] or improved waveguides [26].

3.2.2. Prototypes

Based on the above modeling results, we selected three NC luminophores and one organic dye to fabricate LSCs by dispersing them in a Kraton-based resin, which is a polystyrene (PS), with similar properties as PMMA. The core/shell NCs were $\text{CuInS}_2/\text{ZnS}$, $\text{InP}/\text{ZnSe}/\text{ZnS}$, $\text{CdSe}/\text{CdS}/\text{ZnS}$, and the dye was Lumogen Red dye. The slurry was then doctor-bladed on top of a $50 \times 60 \times 0.6 \text{ cm}^3$ PMMA slabs purchased from Arkema (Altuglas). An identical PMMA slab was placed on top of the doctor-bladed film to encapsulate the luminophore-containing $50 \mu\text{m}$ thin Kraton layer, see Figure 14 for the sandwich structure of the LSC. The fifth device, the blank, was prepared following the same procedure but without a luminophore in the Kraton layer. The assembled LSCs were cut to $45 \times 50 \text{ cm}^2$ to be tested in an outdoor testing facility. Four CIGS photovoltaic (PV) strips (10 cells of 4.51 cm^2 in series, from Miasole/Lusoco, Figure 15) were coupled to each side of the LSCs with a transparent double-sided acrylic tape. The acrylic tape is transparent to the emitted photons by the luminophores, see Figure S3. Similarly, the CIGS strips have maximum external quantum efficiency in the same range, optimizing the performance of the

device, see Figure 16. The geometrical concentration ratio of the LSC is found by dividing the area of the plate by the total area of the cell strips used, i.e., it is 12.5.

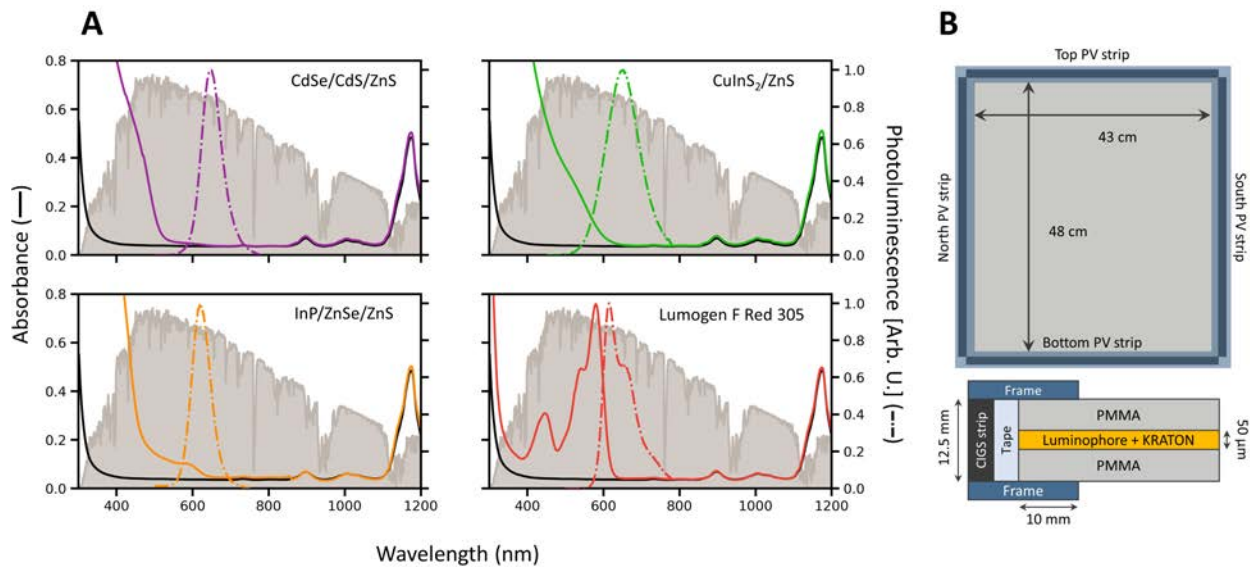


Figure 14. (A) Absorption and emission spectra of the luminophore containing LSCs. The absorption spectrum of the blank LSC is shown in black and the AM 1.5 solar spectrum in grey. (B) The front and side view of the fabricated LSCs. From reference [20].

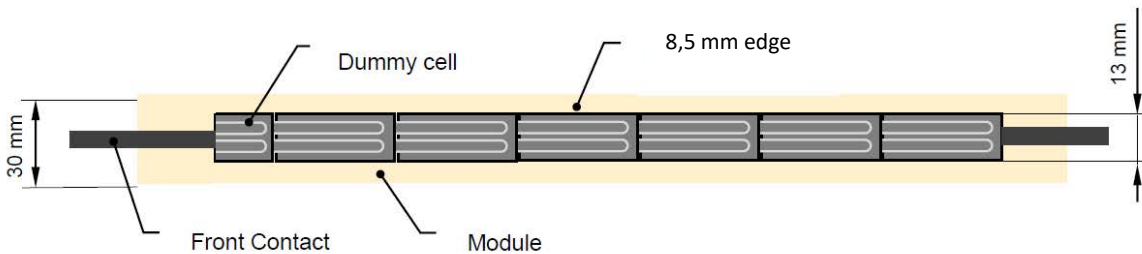


Figure 15. Design of encapsulated CIGS solar cells of 13 mm cell width and length to be customized in multiples of 45 mm (design from Lusoco using cells from Miasole).

The absorption and emission spectra of the LSCs are shown in Figure 14A. The absorbance was measured using the unhindered light beam as the reference. Hence, the minimum absorbance value is 0.08 (92% of transmission) because of reflection losses.

Note that the effective area of the LSC is 43 x 48 cm² for the outdoor measurements since the support frame blocks 1 cm at the edges of the LSC. For the indoor measurements that were performed using Standard Test Conditions, this blockage of the support structure was not present.

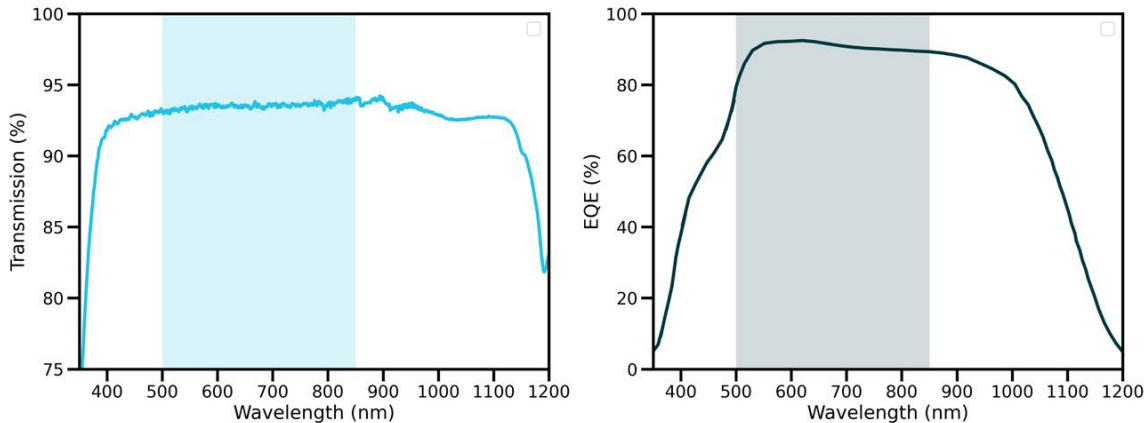


Figure 16. (A) Transmittance of the acrylic tape used to couple the LSC to the PV strip. (B) The external quantum efficiency of the used CIGS PV strips. The shaded areas correspond to the range of emitted photons (500-850 nm) by the luminophores.

Also, small-size 5x2 cm² prototypes containing CuInS₂ or CsPbBr₃ nanocrystals were fabricated in PMMA and Poly(lauryl methacrylate) (PLMA) to optimize the loadings. However, the luminescence of the luminophores was quenched in 10-15 days. Currently, design efforts are focusing on polymeric matrices with higher NCs solubility and the capability to preserve and even enhance the PLQY of the nanocrystals [27]. This is achieved by using polymers with binding motives like thiol, amine, and carboxylic groups.

3.3. Testing

3.3.1. Indoor

Testing under standard test conditions (STC, 1000 W/m², AM1.5 spectrum, 25 °C) of prototypes have been performed at the research facilities of TNO. Selected results from I-V measurements are shown in Table 1. All values are averages for the four cells that are used for the five LSCs in which the different luminophores are embedded. Measurements of visible transparency were performed at UU. Under full sun the CIGS cell strip efficiencies are around 13.5% with fill factor of about 71%. These cell strips are from a lot of 100 pieces, and care was taken to have similar cell efficiencies for each LSC. Notably, the shunt resistance values differ considerably, which will influence the low-light intensity response of the cell strips [28].

The aesthetics properties (AVT) of the devices were determined by absorption spectroscopy. Moreover, the absorption and fluorescence of the device was mapped to assess the homogeneity quality of the coating, which was found to be excellent.

Table 1: Individual data of the cell strips used. The strip STC efficiency (PCE, %) is the efficiency of the CIGS PV strip measured at STC. Fill factor and shunt resistance are also determined at STC. The PCE of the LSC (%) is the PCE of the PV strip as found during STC conditions of the complete LSC. All data are averaged over the four cell strips used per LSC.

LSC luminophore	PCE strip (STC) (%)	FF (STC) (%)	Shunt resistance (STC) (Ohm)	PCE strip (in LSC) (%)	AVT (%)
Lumogen	13.19	71.38	850.3	0.1498	40
CuInS	13.42	71.20	735.2	0.1055	67
CdSe	13.75	70.74	734.9	0.1265	85
InP	13.26	71.02	1075.4	0.0540	78
Blank	13.09	70.85	865.3	0.0375	92

When the LSC is measured under full sun the PCE of the whole device is about two orders of magnitude lower than the cell strip efficiencies when measured directly under full sun (Table 1). This obviously is due to the aperture area of the LSC, which is much larger than the area of the cell strips (geometrical ratio of 12.5), but also due to the different amount of absorbed and emitted photons. The lower the AVT, the higher the intensity of light impinging on the solar cell strips will be. With high AVT, intensity will be low, and in addition the low light response of the cell strips due to the shunt resistance will be more important in determining the low efficiency of the whole device.

The Lumogen LSC showed to have the highest PCE value due to its characteristic bright emission and broad absorption across the solar spectrum [29]. The second-best performer was the CdSe LSC, despite having a higher AVT than CuInS₂ and InP LSCs. We attributed this to the weak absorption at wavelengths longer than 500 nm and higher luminescence efficiency. The third highest efficiency was found for the CuInS₂ LSC. The LSC with the lowest efficiency was the InP LSC. Obviously, the blank LSC performed worse than any of the other devices, but has a non-zero efficiency, as the LSC concentrates a small fraction of the light on the cell strip.

Comparing the obtained PCE values to similar devices reported in literature is difficult. Most research either concerns smaller devices or does not report PCE values [30]. Notably, a 50x50 cm² LSC based on DTB and DPA organic dye molecules with a PCE of 1.03% is reported, however some essential information, such as AVT is missing to allow for a detailed comparison [31].

3.3.2. Outdoor

Outdoor testing of prototypes was performed at Heijmans in Rosmalen, the Netherlands [32]. The fabricated LSC plates were mounted vertically in an aluminum frame and subsequently placed 5 m above ground on top of a solar noise barrier test setup (Figure 17A) in a North–South orientation (Figure 17B). Each cell strip was attached to an EKO Europe IV-tracer via two 12-channel multiplexers using 25 m-long cabling. Full I–V curves were measured every 2 min. Furthermore, a pyranometer was placed nearby to measure global horizontal irradiance (GHI).



Figure 17. A) Test setup in Rosmalen, The Netherlands, the tinted rectangles at the top of the structure are the LSCs described in this report. B) The orientation of the LSC support structure, the numbers correspond to the following luminophores: 1) InP, 2) CuInS₂, 3) CdSe, 4) Lumogen, 5) Blank. The red arrow of the compass at the top left of the picture points toward the geographical North.

A cloudy day (6 February 2021) and a sunny day (24 February 2021) are presented as examples of the analysis of daily performance fluctuations of the LSCs. Cloudy days are characterized by predominantly diffuse irradiance and sunny days by direct irradiance. Figure 18 shows the calculated efficiencies. It is evident that for both days, the LSC with CuInS₂ NCs performs the best, followed by the ones with Lumogen and CdSe NCs inside, and the worst efficiencies are obtained for the InP-based LSC. The blank

LSC shows little-to-no power output. Note that timesteps with $GHI \leq 15 \text{ W/m}^2$ have been removed to avoid outliers.

Figure 18A shows the efficiency on a cloudy day. Since the irradiance is incident as from an isotropically emitting half-sphere, the irradiance, while fluctuating, stays mostly constant over the day. The support structure seems to have little influence on the efficiency of the LSCs during the cloudy day.

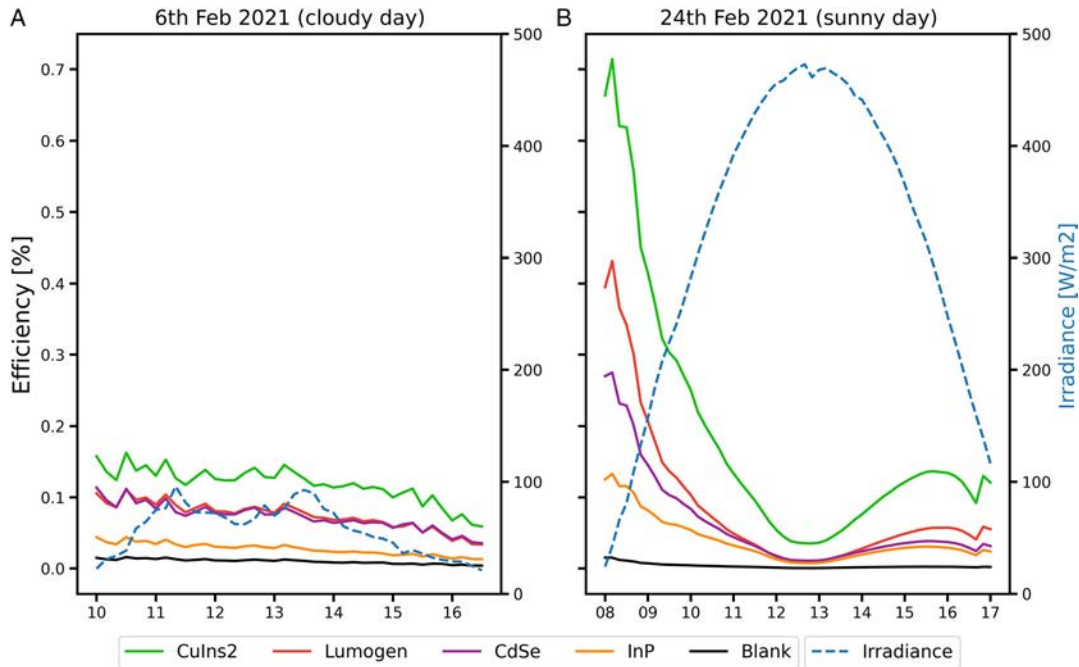


Figure 18. Efficiency of the LSCs during a A) cloudy day and B) a sunny day. The blank LSC without a luminophore is indicated by the black line. The blue dashed line indicates GHI on both days.

In contrast, for the sunny day, Figure 18B, the support structure has a clear effect. At noon, the support structure blocks the direct irradiance on the LSC since it is oriented along the North–South line. The highest efficiencies are obtained in the morning and afternoon when irradiance directly impinges on the LSC (from the East in the morning and the West in the evening). Notable is the similarity between the average efficiencies of the cloudy and sunny day: the average efficiencies for the luminophores for the cloudy and sunny day are, respectively, CuInS₂: 0.118% and 0.184% ($\sigma = 0.024$ and 0.17), Lumogen: 0.07% and 0.09% ($\sigma = 0.019$ and 0.10), CdSe: 0.072% and 0.062% ($\sigma = 0.018$ and 0.067), and InP: 0.027% and 0.038% ($\sigma = 0.0084$ and 0.031). Standard deviation in the main is indicated with σ . The similarity of LSC efficiencies for cloudy and sunny days is unlike conventional PV, for which a clear drop in performance under diffuse irradiance is typically observed. The individual power outputs for the PV strips are further analysed to investigate the effect of irradiance.

The selected date of the cloudy and sunny day was purposely early in the experiment to avoid the effect of degradation of the luminophores. Figure 19 shows the weekly and monthly average efficiency of the luminophores over a year. It is clear that the change in efficiency is highly dependent on the luminophore. The efficiencies for CuInS₂ and InP LSCs both increase in the summer, while the efficiency of the Lumogen and CdSe LSCs decreases quickly after their inception in February. Outdoors, the LSCs are exposed to UV light, temperature changes, and moisture that can cause degradation of the luminophores and the waveguides. Environmental factors could explain the decrease in performance but cannot account for the improvements observed.

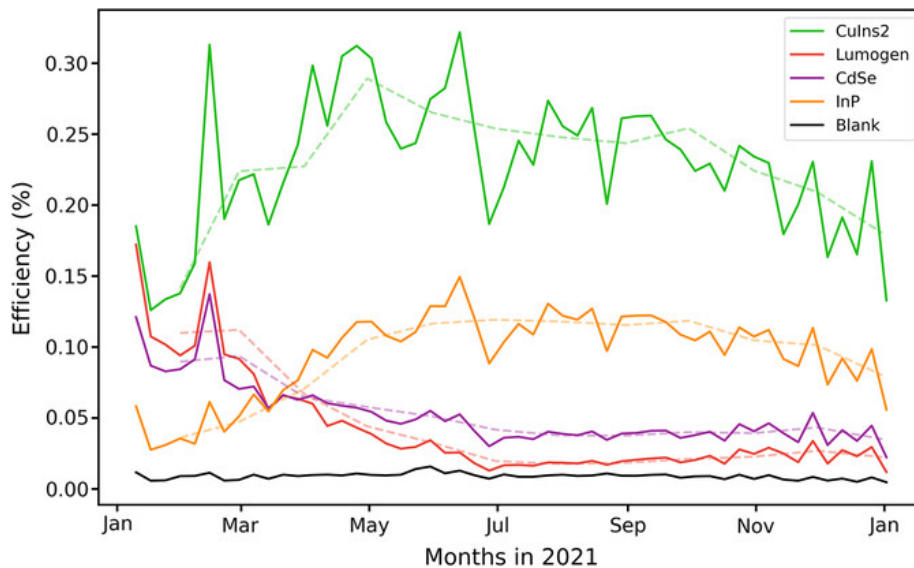


Figure 19. Monthly (dashed line) and weekly (solid line) average efficiency over a year for all the luminophores and the blank LSC.

The increase in efficiency for CuInS₂ and InP potentially results from higher irradiance during summer. Low irradiance values are associated with low efficiencies for conventional PV cells [28], especially since shunt resistances are not very high. However, the temperature increase during summer will have an inverse effect on the efficiency of the PV strips.

A third possibility is the photobrightening of the QDs because of filling the thermodynamic unfavorable defect states. Figure 20 shows the normalized efficiency, relative to that of 17 January 2021 (the start of the experiments), and shows a significant increase in efficiency of 180% and 300% for CuInS₂ and InP, respectively. To investigate this effect, a laboratory study on photodegradation was conducted.

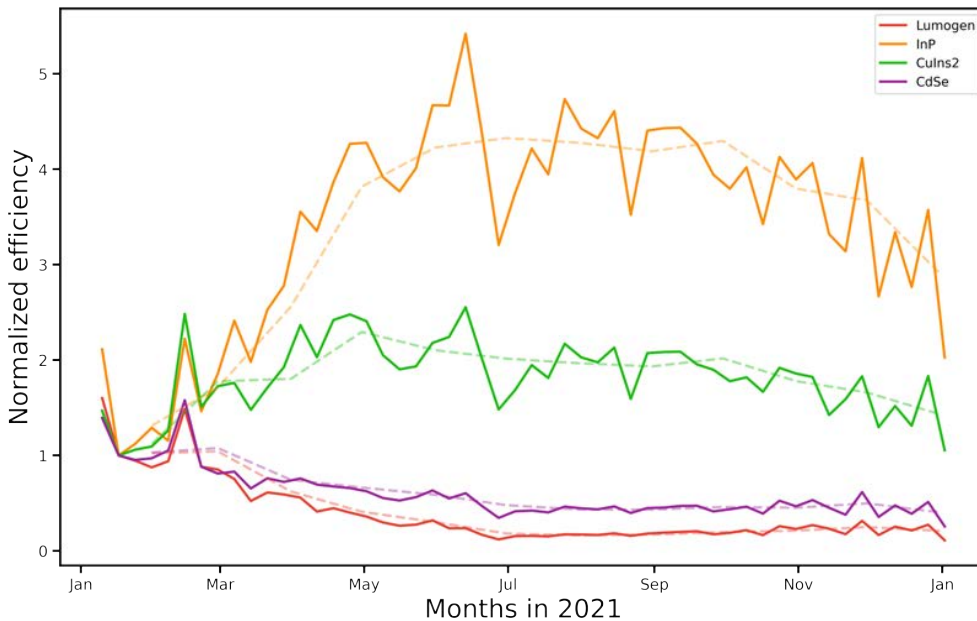


Figure 20. Efficiency of the LSCs normalized by their efficiency on 17th of January 2021.

To test the hypothesis of degradation and photobrightening of the luminophores, small leftover pieces kept in the dark for two years were exposed to white LEDs, and their optical properties were measured over time. The luminescence measured for the InP and CuInS₂ LSCs changed before the white light illumination. For that reason, the earliest measurement under illumination (1.5 h) was taken as the reference value. Within the first 24 h, the luminescence of all three NC filled LSCs increased with respect to their intensity after 1.5 h of illumination (Figure 21A). For the Lumogen LSC, there is 11 % reduction in luminescence. At longer times, the luminescence of CuInS₂ and InP kept increasing up to 1.7 and 4.0 times, respectively (Figure 21B). The initial enhancement observed for the CdSe LSC reversed after one day of illumination, decreasing to 70% of the initial value after 420 h. The performance of the Lumogen LSC consistently decreased during the experiment. The luminescence is the driving force of an LSC and is directly related to the efficiency of the device. The trends observed in the photodegradation experiment qualitatively match the outdoor performance evolution (Figure 22).

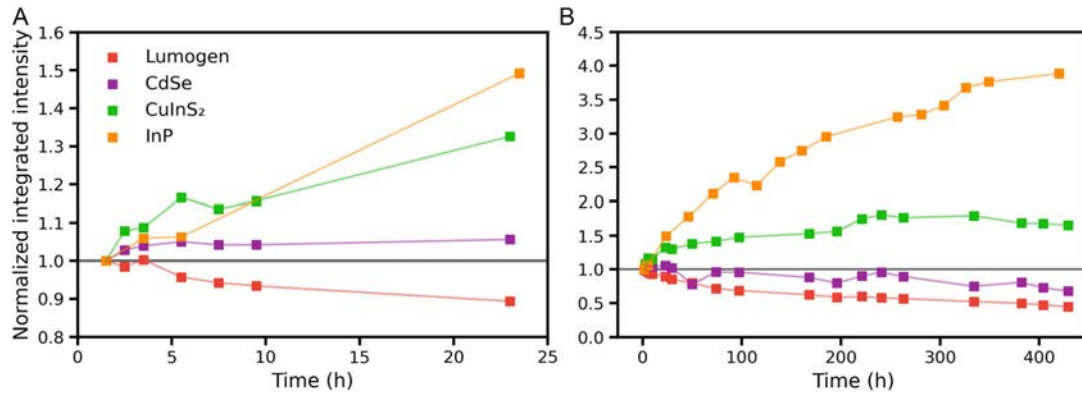


Figure 21. Integrated luminescence intensity normalized by the measured intensity after 1.5 h of illumination. A) First 24 h of illumination. B) Full extension (420 h) of the experiment.

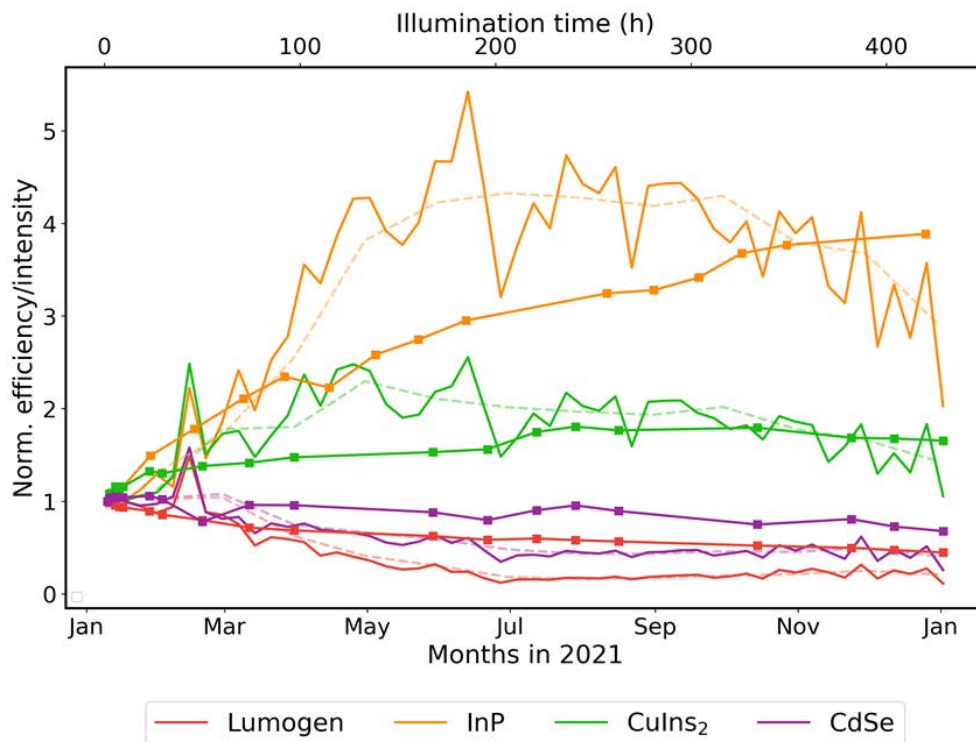


Figure 22: Normalized LSC efficiency (solid and dashed lines) overlapped with the luminescence intensity measured during the photodegradation experiment (solid lines with markers). The bottom x axis corresponds to the outdoors time exposure and the top axis to the exposure time under white light illumination. Note the difference in time scales.

To understand the changes observed in the photodegradation experiment we investigated the evolution of the absorption and emission spectra. We found that during illumination, the characteristic absorption band of PMMA at 1174 nm remains unchanged in all the LSCs, proving that PMMA has not degraded. Lumogen is the only luminophore whose characteristic absorption band decreased over time, a signature

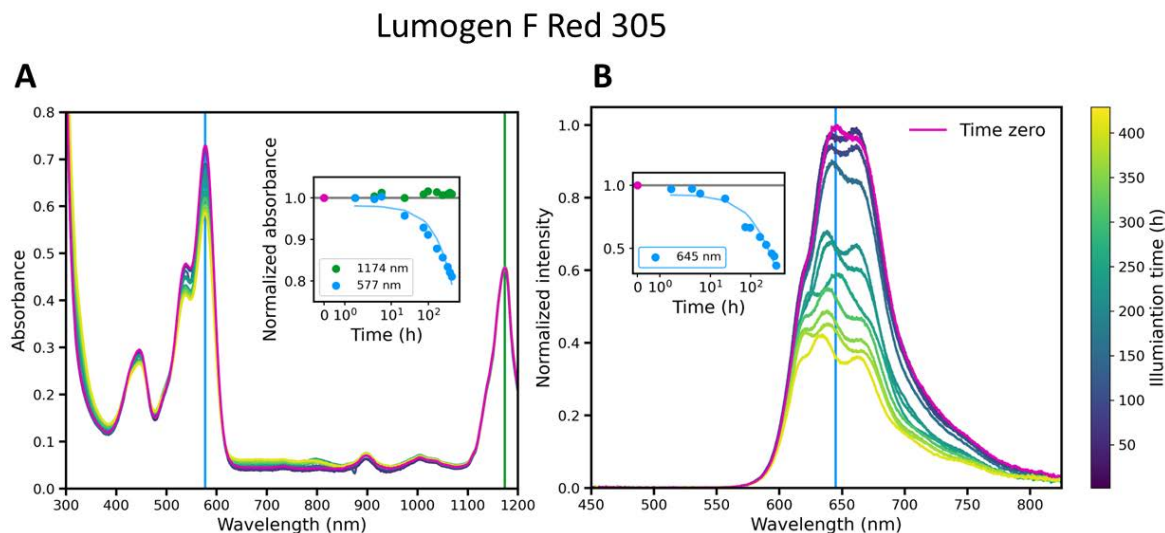


Figure 23. Absorption (left) and emission (right) spectra of the Lumogen F Red 305 LSC measured in the photodegradation experiment. The fluctuations in emission peak position are attributed to etaloning effects. The sample was measured after 1.5, 3.5, 5.5, 23, 74, 97, 168, 241, 334, 382, and 429 h of illumination. Left inset: Temporal evolution of the absorbance at 577 nm (Lumogen F Red 305) and 1174 nm (PMMA) normalized by their values at 1.5 h. Right inset: Time evolution of the PL intensity at 645 nm normalized by its values at 1.5 h. The solid lines in the insets correspond to a single exponential fit of the data. The pink spectra correspond to the measured absorption and emission before the photodegradation experiment was initiated.

of photodegradation (Figure 23). Interestingly, the absorption and emission reductions have a decay rate of 2010 ± 328 and 445 ± 65 h, respectively. The dye degradation occurs slower than the luminescence quenching. Minor photon-induced chemical modifications of Lumogen with the embedding matrix could explain the preservation of the optical transition's intensity while increasing the nonradiative decay rate. Despite having a slower photodegradation rate than similar organic dyes [33] it is evident that Lumogen can photodegrade when embedded in a polymeric matrix [34-37]. It is noteworthy that Lumogen can degrade even in the absence of UV light [34-36] or laser pulses [37].

All NC filled LSCs show no decrease in absorbance after 420 h of illumination, indicating that the QDs have not degraded. It is known that the luminescence of QDs can be enhanced or quenched upon illumination, respectively, known as photobrightening and photodarkening [38]. In the case of CdSe, the initial luminescence increase and subsequent decrease occur at a constant spectral shape (see [32]). The absence of a blueshift when quenched excludes photo-oxidation of the NCs as the cause [39.] Instead, the luminescence quenching can be explained by the increasing fraction of QDs in a dark state [38].

Regarding the InP and CuInS₂ NCs, their response to prolonged light exposure is considerably less studied than for CdSe NCs. The InP and CuInS₂ LSCs experienced a drop in luminescence after 1.5h of white light illumination. To ensure the luminescence measurements had a small impact on the photodegradation process, a halogen lamp with a weak blue light component was used as the excitation source. This approach resulted in stable luminescence spectra for all the samples, including time zero measurements. The luminescence intensity of the InP LSC initially dropped by 10 % and rapidly recovered and increased above the initial value, with constant peak position [32]. The emission spectra show a weak and broad band above 700 nm that is attributed to emission from a trap state [40]. Interestingly, the intensity of this feature decreases during illumination, suggesting that charge carrier traps are being filled or removed. At the ensemble level, photobrightening of InP/ZnSe/ZnS QDs was reported [41], although for only 15 min before quenching and blueshifting start. The constant peak position observed here suggests that the NCs are not degrading. At the single-particle level, it has been found that under continuous illumination, the fraction of InP/ZnS QDs in the bright state increases over time, providing evidence of photobrightening in this material [42].

In contrast to the InP LSC, the initial luminescence drop of 50% observed for the CuInS₂ LSC is not fully recovered in the photobrightening phase (Figure 24). The initial drop in intensity is accompanied by a peak blueshift of 5.5 nm (17 meV). At constant illumination, the luminescence increases, and its maximum is redshifted by 9 nm (27 meV). The NCs' ensemble inhomogeneities can explain this result. Since their optoelectronic properties strongly depend on the size, any size-sensitive transformation will affect smaller and larger NCS within the ensemble differently. Nevertheless, the origin of the photodarkening and photobrightening observed in the NC filled LSCs is not yet fully understood and will be the subject of follow-up studies.

CuInS₂/ZnS

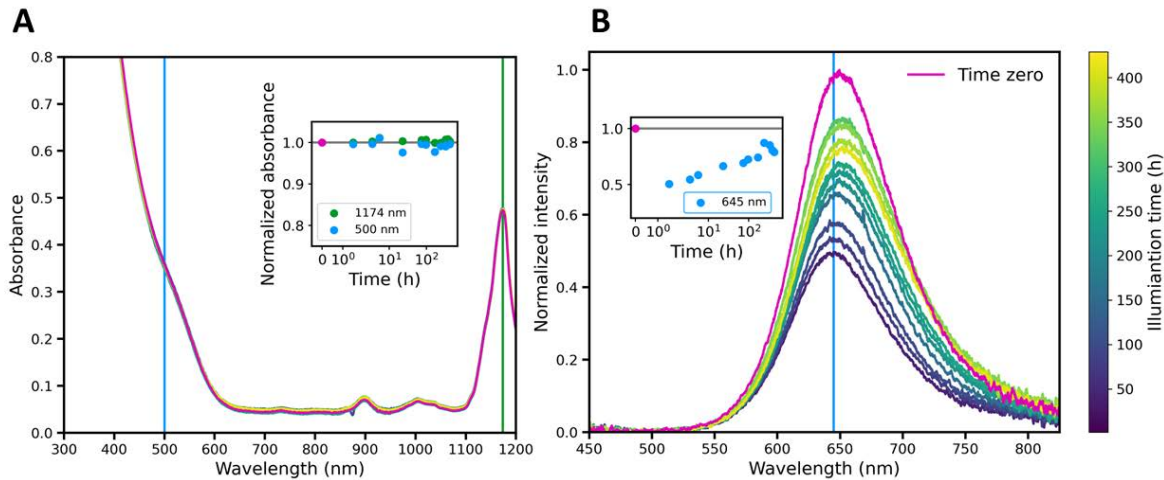


Figure 24. Absorption (left) and emission (right) spectra of the CuInS₂/ZnS LSC measured in the photodegradation experiment. The sample was measured after 1.5, 3.5, 5.5, 23, 74, 97, 168, 241, 334, 382, and 429 h of illumination. Left inset: Temporal evolution of the absorbance at 500 nm (CuInS₂/ZnS) and 1174 nm (PMMA) normalized by their values at 1.5 h. Right inset: Temporal evolution of the PL intensity at 645 nm normalized by its values at 1.5 h. The pink spectra correspond to the measured absorption and emission before the photodegradation experiment was initiated.

4. Discussion

TES-W was an ambitious project with innovative and challenging objectives given the available budget. It was even more challenging when the Covid pandemic hit the world. This hampered experimental work due to restrictions. In addition, in the course of the project, partner Physee realised that they had been too optimistic about the actual TRL level of their technology, although it was based on their patent [43]. The intended NC development at Physee was based on $\text{Ba}_3(\text{PO}_4)_2:\text{Mn}^{5+}$ NCs, which have broad absorption with limited self-absorption. The use of these NCs in LSCs should have the potential of 5-6% PCE, if the PLQY would be 75%, in combination with solar cells with EQE of >75% at the emission wavelength of 1200 nm. This excludes the use of silicon solar cells, and CIGS solar cells with proper bandgap (lower than 1 eV). PLQY values of the barium phosphate particles larger than 30% were not successful, which also prompted Physee to stop the development of coatings with these particles. This has led to a change in business strategy in which the new focus of Physee was the further commercial development of their intelligent windows as part of their SENSE portfolio. The development of LSCs as part of energy harvesting windows is still of interest though. A separate company Fotoniq has been set-up that markets a so-called PAR+ sprayable coating on greenhouse glass that brings diffusivity inside the greenhouse year-round without losing grow light (PAR), which would even enhance profit per hectare greenhouse.

Using the presently available information on NCs, the apparent maximum PCE is around 1%, when one uses the transparency and colour rendering constraints of AVT > 55% and CRI > 70. This is large contrast with values of about 10% for NCs with ideal properties. Significant technological breakthroughs are necessary for LSCs to become economically viable which happens, as speculated, around the 5% efficiency mark. This involves development of NCs with wider absorption, higher PLQY (e.g., quantum cutting), zero self-absorption, but also improved waveguides. In addition, design of solar cells that have high efficiency at low-light intensity, hence very high shunt resistance, would be necessary to harvest all photons that impinge on the LSC sides. Electrical connections and power optimization per LSC are other engineering improvements that will help increase LSC efficiency.

5. Follow up activities

The TES-W project has resulted in a number of important findings. Efficient nanocrystals have been developed, and earlier batches of them have been used to make prototypes that have been tested indoor and outdoors. Especially outdoor tests are rarely performed, and they provided important results on how efficiencies of LSCs change, i.e. increase, decrease, or remained constant depending on weather conditions. Computer simulations showed that with present information on nanocrystals a maximum LSC efficiency of about 1% is possible with high transparency and high colour rendering index. Luminophore improvements together with improved solar cell design would be needed to reach higher efficiencies.

In the MOOI-BIPVT project, which is running from January 2021 to December 2025, the results from the TES-W project are used to further develop LSC-based windows. Furthermore, UU is in close contact with other Dutch groups working on LSCs, i.e., the groups of Michael Debije and Angele Reinders at TU Eindhoven, and the group of Erik van der Kolk at TU Delft, with the purpose of setting up a national working group on LSC research and development. Regarding dedicated solar cell development, collaboration with TNO on CIGS thin film cells will be pursued. Once TRL levels are sufficiently high, collaboration with companies such as Physee and ClearVue [44] will be intensified.

6. Dissemination

Dissemination activities have aimed to promote non-confidential results obtained within the project as swiftly and effectively as possible for the benefit of the whole (scientific) community and to avoid duplication of R&D efforts.

Published papers

- W.G.J.H.M. van Sark, A. Meijerink, R.E.I. Schropp, *Nanoparticles for Solar Spectrum Conversion*, Chapter 12 in *Quantum & Nano Technology for Photovoltaics*, 2nd Edition (L. Tsakalacos, Ed.), Taylor and Francis, Boca Raton, FL, USA, 2024, pp. (in press) (invited)
- Annick Anctil, Meghan N. Beattie, Christopher Case, Aditya Chaudhary, Benjamin D. Chrysler, Michael G. Debije, Stephanie Essig, David K. Ferry, Vivian E. Ferry, Marina Freitag, Isaac Gould, Karin Hinzer, Harald Hoppe, Olle Inganäs, Lethy Krishnan Jagadamma, Min Hun Jee, Raymond K. Kostuk, Daniel Kirk, Stephan Kube, Minyoung Lim, Joseph M. Luther, Lorelle Mansfield, Michael McGehee, Duong Nguyen Minh, Preeti Nain, Matthew O. Reese, Angèle Reinders, Ifor D. W. Samuel, **Wilfried van Sark**, Hele Savin, Ian R. Sellers, Sean E. Shaheen, Zheng Tang, Fatima Toor, Ville Vähänissi, Ella Wassweiler, Emily L. Warren, Vincent R. Whiteside, Han Young Woo, Gang Xiong, and Xitong Zhu, *Status report on emerging photovoltaics*, SPIE Journal of Photonics for Energy (JPE) 13 (2023) 042301 ([10.1117/1.JPE.13.042301](https://doi.org/10.1117/1.JPE.13.042301)).
- Wilfried G. J. H. M. van Sark, Thomas A. de Bruin, Raimon Terricabres-Polo, Celso de Mello Donegá, *Strategies for the optimization of color neutral, transparent, and efficient luminescent solar concentrators*, Proc. SPIE 12668, New Concepts in Solar and Thermal Radiation Conversion V, 2023, 1266802. ([doi:10.1117/12.2676273](https://doi.org/10.1117/12.2676273))
- T.A. de Bruin, W.G.J.H.M. van Sark, *Optimization of Quantum Dot Luminescent Solar Concentrator Single, Double and Triple Structures: a Ray Tracing Simulation Study (FG-6:L02)*, Ceramics International 49 (2023) 24454-24468 ([doi:10.1016/j.ceramint.2022.12.084](https://doi.org/10.1016/j.ceramint.2022.12.084))
- Thomas A de Bruin, Raimon Terricabres-Polo, Annanta Kaul, Natalia K Zawacka, Tim Prins, Thomas F J Gietema, Anne C de Waal, Dick K G de Boer, Daniel A M Vanmaekelbergh, Paul Leblans, Stijn Verkuilen, Zeger Hens, Celso De Mello Donega, Wilfried G J H M van Sark, *Analysis of the 1-year outdoor performance of quantum dot luminescent solar concentrators*, Solar RRL 7 (2023) 202201121 ([doi:10.1002/solr.202201121](https://doi.org/10.1002/solr.202201121))
- Thomas A. de Bruin, Wilfried G.J.H.M. van Sark, *Numerical method for calculation of power conversion efficiency and colorimetrics of rectangular luminescent solar concentrators*, Solar RRL 7 (2023) 202200787 ([doi:10.1002/solr.202200787](https://doi.org/10.1002/solr.202200787))
- Thomas A. de Bruin, Wilfried G.J.H.M. van Sark, *Optimising Absorption in Luminescent Solar Concentrators constraint by Average Visible Transmission and Color Rendering Index*, Frontiers in Physics - Optics and Photonics 10 (2022) 856799. ([doi:10.3389/fphy.2022.856799](https://doi.org/10.3389/fphy.2022.856799))
- Chenchen Yang, Harry A. Atwater, Marc A. Baldo, Derya Baran, Christopher Barile, Miles C. Barr, Matthew Bates, Mounqi G. Bawendi, Matthew R. Bergren, Christoph J. Brabec, Sergio Brovelli, Vladimir Bulović, Paola Ceroni, Michael G. Debije, Jose-Maria Delgado-Sanchez, Wen-Ji Dong, Phillip M. Duxbury, Rachel C. Evans, Stephen R. Forrest, Daniel R. Gamelin, Noel C. Giebink, Xiao Gong, Gianmarco Griffini, Fei Guo, Christopher K. Herrera, Anita W.Y. Ho-Baillie, Russell J.

Holmes, Sung-Kyu Hong, Thomas Kirchartz, Hongbo Li, Yilin Li, Dianyuan Liu, Maria A. Loi, Christine K. Luscombe, Nikolay S. Makarov, Fahad Mateen, Raffaello Mazzaro, Hunter McDaniel, Michael D. McGehee, Francesco Meinardi, Amador Menéndez-Velázquez, Jie Min, David B. Mitzi, Jun Hyuk Moon, Andrew Nattestad, Mohammad K. Nazeeruddin, Ana Flavia Nogueira, Ulrich W. Paetzold, David L. Patrick, Andrea Pucci, Barry P. Rand, Elsa Reichmanis, Bryce Sydney Richards, Jean Roncali, Federico Rosei, Timothy W. Schmidt, Franky So, Chang-Ching Tu, **Wilfried G.J.H.M. van Sark**, Rafael Verduzco, Alberto Vomiero, Wallace W. H. Wong, Kaifeng Wu, Hin-Lap Yip, Xiaowei Zhang, Haiguang Zhao, Richard R. Lunt, *Consensus Statement: Standardized Reporting of Power-Producing Luminescent Solar Concentrator Performance*, *Joule* 6 (2022) 1-15. ([doi:10.1016/j.joule.2021.12.004](https://doi.org/10.1016/j.joule.2021.12.004)).

- J.C. Goldschmidt, W.G.J.H.M. van Sark, *Luminescent Solar Concentrator*, Chapter 1.26 in W.G.J.H.M. van Sark, V. Fthenakis (Eds.) *Photovoltaic Technology*, Volume 1 in T. Letcher (Ed.) *Comprehensive Renewable Energy 2nd Edition*, Elsevier, United Kingdom, 2022, pp. 561 – 581. ([doi:10.1016/B978-0-12-819727-1.00145-X](https://doi.org/10.1016/B978-0-12-819727-1.00145-X)).

Conference contributions

- Thomas A. de Bruin, Wilfried G.J.H.M. van Sark, *Simulation-assisted outlook for luminescent solar concentrators with >5% power conversion efficiency and appropriate transmission*, 40th EU PVSEC Lisbon 18-22 September 2023 (poster, 4BV.4.2)
- Raimon Terricabres-Polo, Celso de Mello Donega, *Quantum Dot based Luminescent Solar Concentrators: Performance and Stability*, IUPAC-CHAINS, The Hague, 21-25 August 2023
- Wilfried G. J. H. M. van Sark, Thomas A. de Bruin, Raimon Terricabres-Polo, Celso de Mello Donegá, *Strategies for the optimization of color neutral, transparent, and efficient luminescent solar concentrators*, SPIE Optics and Photonics conference, San Diego, 20-24 August 2023 (invited oral).
- Raimon Terricabres-Polo, Celso de Mello Donega, *Photobrightening and photodarkening of Quantum Dots*, Exciting Nanoparticles Summer School, Bad Honnef, 31 July – 4 August 2023
- Raimon Terricabres-Polo, Huygen J Jöbssis, P Tim Prins, Eline M Hutter, Celso de Mello Donega, *Evidence of long-lived delocalized electrons in CuInS₂/CdS nanocrystals*, NANAX 10, Klosterneuburg, 3-7 July 2023
- Raimon Terricabres-Polo, Celso de Mello Donega, *Photobrightening and photodarkening of Quantum Dots*, LMPV Symposium, Amsterdam, 16 June 2023
- Wilfried van Sark, Thomas de Bruin, *Outdoor performance of nanocrystal luminescent solar concentrators*, SHIFT22 (Spectral sHapIng For biomedical and energy applicaTions – 2022), Tenerife, 10-14 October 2022 (oral)
- Thomas de Bruin, Natalia Zawacka, Anne de Waal, Stijn Verkuilen, Tim Prins, Celso de Mello Donegá, Paul Leblans, Zeger Hens, Daniel Vanmaekelbergh, Wilfried van Sark, *1-year outdoor performance test results of luminescent solar concentrators with embedded nanocrystals*, 8th World Conference on Photovoltaic Energy Conversion (WCPEC-8), Milano, Italy 26-30 September 2022 (oral)
- Raimon Terricabres-Polo, Katarina Condric, Celso de Mello Donega, *Size-, shape-, and composition-controlled wurtzite CuInS₂ nanocrystals by partial Cu⁺ for In³⁺ cation exchange*, GRC Semiconductor nanocrystals, Les Diablerets, 4-8 July 2023

- T.A. de Bruin, W.G.J.H.M. van Sark, *Optimization of Quantum Dot Luminescent Solar Concentrator Single, Double and Triple Structures: a Ray Tracing Simulation Study (FG-6:L02)*, CIMTEC2022, Perugia, 26-29 June 2022.

Student reports

- Alessandro di Biasi, *Numerical model for calculation of key performance indicators of quantum cutting perovskite-based luminescent solar concentrators*, MSc Thesis, UU, 2023.
- Madhu Ganpat, *Impact of surface chemistry, size and crystal structure on Cu⁺ for Ga³⁺ cation exchange in CuInS₂ nanocrystals*, BSc thesis, UU, 2023.
- Liselotte Nass, *Near-Infrared emitting Yb³⁺-doped CsPbX₃ (X = Cl, Br) perovskite nanocrystals for Luminescent Solar Concentrators*, MSc Thesis, UU, 2022
- Ruben van der Vliet, *Synthesis and post-synthetic modifications of CuInS₂ nanocrystals*, MSc thesis, UU, 2022
- Maryam Sadeqi, *CuInS₂/ZnS Nanocrystals for Luminescent Solar Concentrators*, BSc Thesis, UU, 2022.
- Katarina Condric, *Tailoring cation exchange in nanomaterials*, MSc Thesis, UU, 2022.
- Thomas Gietema, *Investigating The Long-term Efficiency And Degradation Of Luminescent Solar Concentrators*, MSc Thesis, UU, 2022.

PR of project and further PR possibilities

The project partners would like to be approached for any further publicity activities and would like to contribute to public activities of the Rijksdienst voor Ondernemend Nederland or the TKI-Urban Energy and are happy to add these insights to the debate about the energy transition in the Netherlands.

References

- [1] P. Corti, P. Bonomo, F. Frontini, P. Macé, E. Bosch, *Building Integrated Photovoltaics, a practical handbook for solar buildings' stakeholders, Status Report 2020*, SUPSI, Becquerel Institute, 2020.
- [2] C.J. Traverse, R. Pandey, M.C. Barr, R. R. Lunt, *Emergence of highly transparent photovoltaics for distributed applications*, *Nature Energy* 2 (2017) 849 – 860.
- [3] F. Meinardi, H. McDaniel, F. Carulli, A. Colombo, K.A. Velizhanin, N. S. Makarov, R. Simonutti, V.I. Klimov, S. Brovelli, *Highly efficient large-area colourless luminescent solar concentrators using heavy-metal-free colloidal quantum dots*, *Nature Nanotechnology* 10 (2015) 878 – 886.
- [4] C. Xia, J.D. Meeldijk, H.C. Gerritsen, C. de Mello Donega, *Highly Luminescent Water-Dispersible NIR-Emitting Wurtzite CuInS₂/ZnS Core/Shell Colloidal Quantum Dots*, *Chem. Mater* 29 (2017) 4940 – 4953.
- [5] P. Moraitis, W.G.J.H.M. van Sark, *Visual Appearance of Nanocrystal-Based Luminescent Solar Concentrators*, *Materials* 12 (2019) 885.
- [6] M.G. Debije, C. Tzikas, M.M. de Jong, M. Kanellis, L. H. Slooff, *The solar noise barrier project: 3. The effects of seasonal spectral variation, cloud cover and heat distribution on the performance of full-scale luminescent solar concentrator panels*, *Renewable Energy* 116 (2018) 335 - 343.
- [7] W. van Sark, P. Moraitis, C. Aalberts, M. Drent, T. Grasso, Y. L'Ortije, M. Visschers, M. Westra, R. Plas, W. Planje, *The "Electric Mondrian" as a Luminescent Solar Concentrator Demonstrator Case Study*, *Solar RRL* 1 (2017) 1600015.
- [8] T.J. Milstein, D.M. Kroupa, D.R. Gamelin, *Picosecond Quantum Cutting Generates Photoluminescence Quantum Yields Over 100% in Ytterbium-Doped CsPbCl₃ Nanocrystals*, *Nano Letters* 18 (2018) 3792 – 3799.
- [9] L. Li, A. Pandey, D.J. Werder, J.M. Pietryga, V. Klimov, *Efficient Synthesis of Highly Luminescent Copper Indium Sulfide-Based Core/Shell Nanocrystals with Surprisingly Long-Lived Emission*, *Journal of the American Chemical Society* 133 (2011) 1176–1179
- [10] R. Terricabres-Polo, C. de Mello Donega, *Size-, shape-, and composition controlled wz CuInS₂ nanocrystals by partial Cu⁺ for In³⁺ cation exchange*, *GRC Conference on Semiconductor NCs* (2022).
- [11] S.O.M. Hinterding, A.C. Berends, M. Kurttepel, M.E. Moret, J.D. Meeldijk, S. Bals, W. van der Stam, C. de Mello Donega, *Tailoring Cu⁺ for Ga³⁺ Cation Exchange in Cu_{2-x}S and CuInS₂ Nanocrystals by Controlling the Ga Precursor Chemistry*, *ACS Nano* 13 (2019) 12880–12893.
- [12] E. Yablonoitch, *Thermodynamics of the fluorescent planar concentrator*, *Journal of the Optical Society of America* 70 (1980) 1362.
- [13] A. Chatten, D. Farrel, C. Jermyn, P. Thomas, B. Buxton, A. Buchtemann, R. Danz, K. Barnham, *Thermodynamic modelling of luminescent solar concentrators*, in *Conference Record of the Thirty-first IEEE Photovoltaic Specialists Conference*, 2005, pp. 82–85.
- [14] A.J. Chatten, K.W.J. Barnham, B.F. Buxton, N.J. Ekins-Daukes, M.A. Malik, *Quantum dot solar concentrators*, *Semiconductors* 38 (2004) 909–917.
- [15] S.J. Gallagher, P.C. Eames, B. Norton, *Quantum dot solar concentrator behaviour, predicted using a ray trace approach*, *International Journal of Ambient Energy* 25 (2004) 47–56.
- [16] Synopsis, *Lighttools illumination design software*, (2022).
- [17] D. Farrell, *PVtrace optical ray tracing for luminescent materials and spectral converter photovoltaic devices*, (2020).
- [18] A. Burgers, J. Van Roosmalen, R. and Kinderman, *Modeling of the luminescent concentrators by ray-tracing*, *Proceedings of the 20th European Photovoltaic Solar Energy Conference and Exhibition*, (2005)

- [19] T.A. de Bruin, W.G.J.H.M. van Sark, *Optimization of Quantum Dot Luminescent Solar Concentrator Single, Double and Triple Structures: a Ray Tracing Simulation Study*, *Ceramics International* 49 (2023) 24454-24468.
- [20] T.A. de Bruin, W.G.J.H.M. Van Sark, *Optimising Absorption in Luminescent Solar Concentrators constraint by Average Visible Transmission and Color Rendering Index*, *Frontiers in Physics* 10 (2022) 856799.
- [21] [16] R.R. Lunt, *Theoretical limits for visibly transparent photovoltaics*, *Applied Physics Letters* 101 (2012) 043902.
- [22] I. Sychugov, *Analytical Description of a Luminescent Solar Concentrator Device*, *Optica* 6 (2019) 1046.
- [23] T.A. de Bruin, W.G.J.H.M. Van Sark, *Numerical Method for Calculation of Power Conversion Efficiency and Colorimetrics of Rectangular Luminescent Solar Concentrators*, *Solar RRL* 7 (2023) 2200787.
- [24] M. Sharma, K. Gungor, A. Yeltik, M. Olutas, B. Guzelturk, Y. Kelestemur, T. Erdem, S. Delikanli, J. R. McBride, H. V. Demir, *Near-unity emitting copper-doped colloidal semiconductor quantum wells for luminescent solar concentrators*, *Advanced Materials* 29 (2017) 1700821.
- [25] Y. Zhou, D. Benetti, Z. Fan, H. Zhao, D. Ma, A. O. Govorov, A. Vomiero, F. Rosei, *Near Infrared, Highly Efficient Luminescent Solar Concentrators*, *Advanced Energy Materials* 6 (2016) 1501913.
- [26] K. Park, J. Yi, S.-Y. Yoon, S.M. Park, J. Kim, H.-B. Shin, S. Biswas, G.Y. Yoo, S.-H. Moon, J. Kim, M.S. Oh, A. Wedel, S. Jeong, H. Kim, S.J. Oh, H.K. Kang, H. Yang, C.J. Han, *Luminescent solar concentrator efficiency enhanced via nearly lossless propagation pathways*, *Nature Photonics* 18 (2024).
- [27] A. Marinins, R.Z. Shafagh, W. van der Wijngaart, T. Haraldsson, J. Linnros, J.G.C. Veinot, S. Popov, I. Sychugov, *Light-Converting Polymer/Si Nanocrystal Composites with Stable 60–70% Quantum Efficiency and Their Glass Laminates*, *ACS Applied Materials & Interfaces* 9 (2017) 30267-30272.
- [28] N.H. Reich, W.G.J.H.M van Sark, E.A. Alsema, R.W. Lof, R.E.I. Schropp, W.C. Sinke, W.C. Turkenburg, *Crystalline silicon cell performance at low light intensities*, *Solar Energy Materials and Solar Cells* 93 (2009) 1471-1481.
- [29] G. Seybold, G. Wagenblast, *New perylene and violanthrone dyestuffs for fluorescent collectors*, *Dyes and Pigments* 11 (1989) 303-317.
- [30] J. Roncali, *Luminescent Solar Collectors: Quo Vadis?*, *Advanced Energy Materials* 10 (2020), 2001907.
- [31] N. Aste, L.C. Tagliabue, C. Del Pero, D. Testa, R. Fusco, *Performance analysis of a large-area luminescent solar concentrator module*, *Renewable Energy* 76 (2015) 330-337.
- [32] T.A. de Bruin, R. Terricabres-Polo, A. Kaul, N.K. Zawacka, P.T. Prins, T.F.J. Gietema, A.C. de Waal, D.K.G. de Boer, D.A.M. Vanmaekelbergh, P. Leblans, S. Verkuilen, Z. Hens, C. De Mello Donega, W.G.J.H.M. van Sark, *Analysis of the 1-year outdoor performance of quantum dot luminescent solar concentrators*, *Solar RRL* 7 (2023) 202201121.
- [33] L. R. Wilson, B. S. Richards, *High Efficiency Dyes for Luminescent Solar Concentrators: Photostability and Modeling*, *Proceedings of the 23rd European Photovoltaic Solar Energy Conference and Exhibition*, (2008), 510-512.
- [34] J.-M. Delgado-Sanchez, *Luminescent solar concentrators: {Photo}-stability analysis and long-term perspectives*, *Solar Energy Materials and Solar Cells* 202 (2019) 110134.
- [35] M.G. Hyldahl, S.T. Bailey, B.P. Wittmershaus, *Photo-stability and performance of CdSe/ZnS quantum dots in luminescent solar concentrators*, *Solar Energy* 83 (2009) 566-573.
- [36] G. Griffini, L. Brambilla, M. Levi, M. Del Zoppo, S. Turri, *Photo-degradation of a perylene-based organic luminescent solar concentrator: Molecular aspects and device implications*, *Solar Energy Materials and Solar Cells* 111 (2013) 41-48.

- [37] N. Tanaka, N. Barashkov, J. Heath, W. N. Sisk, Photodegradation of polymer-dispersed perylene di-imide dyes, *Applied Optics* 45 (2006) 3846-3851.
- [38] M.A. Osborne, S.F. Lee, *Quantum dot photoluminescence activation and decay: dark, bright, and reversible populations in ZnS-capped CdSe nanocrystals*, *ACS Nano* 5 (2011) 8295-8304.
- [39] W.G. Van Sark, P.L. Frederix, D.J. Van den Heuvel, H.C. Gerritsen, A.A. Bol, J.N. Van Lingen, C. de Mello Donega, A. Meijerink, *Photooxidation and photobleaching of single CdSe/ZnS quantum dots probed by room-temperature time-resolved spectroscopy* *Journal of Physical Chemistry B* 105 (2001) 8281-8284.
- [40] A. Guzelian, J.B. Katari, A.V. Kadavanich, U. Banin, K. Hamad, E. Juban, A. Alivisatos, R. Wolters, C. Arnold, J. Heath, *Synthesis of size-selected, surface-passivated InP nanocrystals*, *Journal of Physical Chemistry* 100 (1996) 7212-7219.
- [41] F. Dussert, G. Sarret, K. D. Wegner, O. Proux, G. Landrot, P.-H. Jouneau, P. Reiss, M. Carrière, *Physico-Chemical Transformation and Toxicity of Multi-Shell InP Quantum Dots under Simulated Sunlight Irradiation, in an Environmentally Realistic Scenario*, *Nanomaterials* 12 (2022) 3703.
- [42] V. Chandrasekaran, M. D. Tessier, D. Dupont, P. Geiregat, Z. Hens, E. Brainis, *Nearly blinking-free, high-purity single-photon emission by colloidal InP/ZnSe quantum dots*, *Nano Letters* 17 (2017) 6104-6109.
- [43] A. Jung, S. van Overbeek, C. Kao, O. van den Berg, *Inorganic luminescent materials for solar radiation conversion devices*, Patent WO 2019/240578.
- [44] <https://www.clearvuepv.com>